

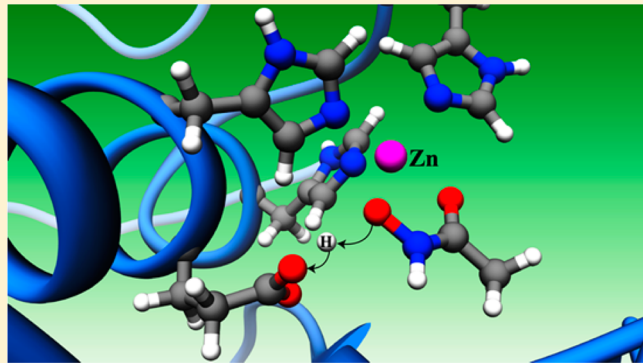
Toward On-The-Fly Quantum Mechanical/Molecular Mechanical (QM/MM) Docking: Development and Benchmark of a Scoring Function

Prasad Chaskar, Vincent Zoete,* and Ute F. Röhrig*

Swiss Institute of Bioinformatics, Molecular Modeling Group, Quartier Sorge, Bâtiment Génopode, CH-1015 Lausanne, Switzerland

Supporting Information

ABSTRACT: We address the challenges of treating polarization and covalent interactions in docking by developing a hybrid quantum mechanical/molecular mechanical (QM/MM) scoring function based on the semiempirical self-consistent charge density functional tight-binding (SCC-DFTB) method and the CHARMM force field. To benchmark this scoring function within the EADock DSS docking algorithm, we created a publicly available dataset of high-quality X-ray structures of zinc metalloproteins (<http://www.molecular-modelling.ch/resources.php>). For zinc-bound ligands (226 complexes), the QM/MM scoring yielded a substantially improved success rate compared to the classical scoring function (77.0% vs 61.5%), while, for allosteric ligands (55 complexes), the success rate remained constant (49.1%). The QM/MM scoring significantly improved the detection of correct zinc-binding geometries and improved the docking success rate by more than 20% for several important drug targets. The performance of both the classical and the QM/MM scoring functions compare favorably to the performance of AutoDock4, AutoDock4Zn, and AutoDock Vina.



1. INTRODUCTION

Computational techniques including docking have become valuable tools for drug design over the last decades.¹ The task of molecular docking is to predict the binding mode of a ligand within the binding site of a target macromolecule, usually an enzyme or a receptor. Docking necessitates the combination of a conformational sampling algorithm, which generates putative ligand poses, with a scoring function to rank the poses. Ideally, the scoring function should accurately capture the free energy of ligand–protein interactions to identify the native binding mode as its global minimum, while, at the same time, being fast to calculate, in order to treat a large number of ligand poses. Force-field based scoring functions, which do not rely on data fitted to currently known ligand–protein complexes, are the most universal and well-suited for systematic improvements.

Main challenges for docking algorithms include the accurate treatment of protein flexibility,² solvation,³ covalent interactions,⁴ and polarization.⁵ The latter two are quantum chemical in nature and can be addressed by quantum mechanical (QM) approaches. Since it would be computationally demanding to describe a large system such as a ligand–protein complex entirely with a traditional QM method, hybrid quantum mechanical/molecular mechanical (QM/MM) methods⁶ are gaining importance in the field of structural biology and drug design.^{7–14} In this multiscale approach, only the region of interest is described with a QM method, which is embedded in a classically described environment. Alternatively,

linear-scaling semiempirical QM methods can be applied to large systems.^{15,16}

The QM method used in a docking algorithm should be chosen according to its accuracy and the available computational resources, allowing to score a large number of ligand binding poses. Semiempirical methods, such as PM6^{16–18} or the self-consistent charge density functional tight binding (SCC-DFTB) approach,^{19–23} are the methods of choice for docking applications. Inclusion of dispersion corrections can further enhance their accuracy.¹⁷ In most studies, including QM information in docking has been found to be advantageous over classical docking, justifying the additional computational cost.^{10,13,14,24}

Information from QM calculations can be included in docking algorithms at different levels. Three approaches of increasing computational demand are (i) the improvement of classical force fields for specific cases; (ii) the rescoring of docking poses with a QM/MM method; and (iii) on-the-fly QM/MM docking.

The first approach, improving the scoring function for a specific case using QM calculations, has been pioneered by the “QM-polarized ligand docking” (QMPLD)²⁵ approach in Glide/QSite, where the ligand charges used for classical docking are obtained from QM/MM charge calculations. For

Received: July 14, 2014

Published: October 9, 2014



application to metalloproteins, it was shown later that it is necessary to also include the metal ion and its protein ligands in the QM subsystem.¹⁰ Similar ligand polarization schemes have also been explored by other groups.^{5,26,27} Beyond the reparameterization of electrostatic interactions, we have shown that ligand–protein interactions in the case of hemoproteins, which are primarily of covalent nature, can be approximated by a Morse-like metal binding potential (MMBP) to achieve increased success rates in docking.⁴ This approach has a relatively low computational cost, but transferability and accuracy are important issues.

The second approach, rescoring a classical docking result with a QM/MM method, captures all quantum effects in ligand–protein binding.¹⁴ However, if the native binding mode is energetically unfavorable in the classical scoring function, it might not be present among the results and, thus, the docking will fail. This approach necessitates more computational resources than the first one, as a few tens to hundreds of solutions usually must be considered.²⁸ In cases for which the correct binding mode is known, QM-informed scoring functions have widely been used for affinity prediction.^{12,29–38}

The most rigorous solution is clearly the third approach, using a QM/MM description of the complex during the docking run, so that the charge distribution and the covalent binding contributions will be determined on the fly for each conformation of the complex during the docking. However, this solution is computationally the most demanding and has not yet been fully exploited. Working toward this aim, in the present study, we develop a semiempirical QM/MM scoring function based on the SCC-DFTB/CHARMM interface,^{21,23,39} which can easily be integrated into our CHARMM-based EADock DSS⁴⁰ docking algorithm. We benchmark this QM/MM scoring function on the description of zinc metalloproteins, using a rescoring approach.

Metal ions such as zinc play an important role for protein structure and function,^{41,42} and many zinc proteins are potential drug targets.^{43,44} The divalent zinc cation induces strong polarization of the active site, which is neglected in fixed-charge classical force fields and poses a problem for many scoring functions.^{10,45–51}

Here, we carefully devised a dataset of zinc metalloprotein complexes limited to druglike ligands and high-quality X-ray structures, characterized by a low diffraction-component precision index (DPI)⁵² and complete and unambiguous ligand coordinates. Since a high success rate for zinc-binding ligands could theoretically be obtained by overemphasizing ligand–zinc interactions, we did not only consider complexes with a ligand directly coordinated to a zinc ion (zinc-binding dataset), but also complexes with a ligand not in direct contact with the Zn ion, although a free coordination site exists (zinc-nonbinding or allosteric dataset). For each complex of the test set, we created an ensemble of 250 ligand poses by classical docking, which was then rescored with different classical and QM/MM models. To eliminate the influence of sampling failures upon the scoring results, we also included the minimized native poses in the ensembles.

In brief, we found that the QM/MM scoring function yielded an improved success rate (77.0% vs 61.5%) for the zinc-binding dataset, while the success rate for the zinc-nonbinding dataset remained constant but was considerably lower (49.1%). The lower success rate for the allosteric test set could be attributed to difficulties in describing very solvent-accessible ligands and to spurious zinc binding. For zinc binders, the QM/MM

scoring function substantially improved the detection of correct zinc-binding geometries from 46.9% to 83.6% and the correct description of tetrahedral complexes from 15.8% to 85.3%. The robustness of the QM/MM scoring function, with respect to the employed solvation model, the size of the QM subsystem, and the influence of the minimization scheme was investigated. For some therapeutically relevant enzyme classes from the zinc-binding dataset such as carbonic anhydrases (CA) and ADAM metalloproteinase domain 17 (ADAM17, also called TACE), the QM/MM approach yielded a substantially higher success rate. For ADAM17 metalloproteinase bound to ligands with a hydroxamic acid functionality, an expanded QM/MM model including the catalytic Glu406 in the QM region reproduced the proton transfer described in the literature,^{29,53,54} upon minimization of the highest ranked binding pose.

Taken together, our results suggest that the increased accuracy of the QM/MM scoring function can be useful for drug design applications.

2. METHODS

2.1. Datasets. In order to benchmark our QM/MM scoring function, we devised a dataset of zinc metalloprotein complexes limited to druglike ligands and high-quality X-ray structures, including both complexes with direct ligand–zinc interaction (zinc binders) and complexes where the ligand does not directly bind to the Zn ion (zinc nonbinders). As a measure of X-ray structure quality, we used the diffraction-component precision index (DPI),⁵² which is calculated using the DPICalc algorithm from Mikko J. Vainio (<http://users.abo.fi/mivainio/shaep/download.php>). We downloaded all complexes containing at least one Zn ion and one other ligand from the RCSB Protein Database⁵⁵ (<http://www.pdb.org>) on May 9, 2012 (7360 complexes) and applied the following filters to them:

- Experimental method: X-ray crystallography
- Quality of the structure: resolution <2.5 Å, DPI <0.5 Å, ligand without missing atoms and alternative conformations⁵⁶
- Complex type: only protein–ligand complexes, no DNA
- Zinc coordination by protein: coordination number = 2–4 and coordination only through side-chain atoms (to avoid backbone cuts in the QM/MM calculations)
- Zinc accessibility: either a bound water molecule or a coordination number of <4
- Active site: no co-factors closer than 8 Å to the ligand
- Ligand requirements for docking: at least five heavy atoms, maximum 16 rotatable bonds, not covalently bound to the protein, not a buffer molecule or a co-crystallizing agent (e.g., tris, glycerol)
- Ligand requirements for QM/MM calculations: availability of classical parameters from SwissParam⁵⁷ and SCC-DFTB parameters from www.dftb.org.^{58–60} Because of the lack of SCC-DFTB parameters for halogens and phosphorus in combination with zinc from this repository, 85 protein–ligand complexes were excluded from the dataset.

We rejected 44 multinuclear zinc protein–ligand complexes because the filter did not allow co-factors within proximity of the ligand. However, these complexes, as well as the DNA complexes, are technically treatable within our approach. Finally, we applied a distance-based criterion to assign each complex to the binding (zinc–ligand separation: 1.75–2.5 Å) or the nonbinding/allosteric (3.3–10 Å) subset. This

Table 1. Zinc-Binding Functionalities (ZBFs) in the Zinc-Binding Dataset^a

zinc-binding functionality, ZBF	charge on ZBF	number of cases	classical success ^b	QM/MM success ^b	PDB IDs
alkanolamine	0	4	3 (75.0%)	3 (75.0%)	1EVK, 1EVL, 1FYE, 3UH0
amide	0	5	5 (100.0%)	5 (100.0%)	2XUM, 3NFZ, 3Q9C, 3Q9E, 3RCQ
amine	0	3	2 (66.7%)	2 (66.7%)	2AFU, 3MF1, 3PAO
carbamodithioic acid	-1	3	3 (100.0%)	3 (100.0%)	3P58, 3PSA, 3PSL
carboxylic acid	-1	17	12 (70.6%)	8 (47.1%)	1J36, 1LRH, 2DVU, 2QDS, 2V77, 2YB9, 3A6J, 3CHQ, 3F28, 3F2P, 3FCQ, 3FGQ, 3FUK, 3FXP, 3KQH, 4A39
hydantoin	-1	3	0 (0.0%)	3 (100.0%)	3L0V, 3LE9, 3LEA
hydroxamic acid	0	26	9 (34.6%)	25 (96.1%)	1BKC, 1IX1, 1RS5, 1Y93, 2A8H, 2DW0, 2FV5, 2FV9, 2G7Q, 2I47, 2IMB, 2J83, 2VES, 2YJ8, 2VQH, 3B7U, 3EDZ, 3EWJ, 3KME, 3L0T, 3P3C, 3P6, 3PN4, 3U04, 3UIY
hydroxyl	0	56	49 (87.5%)	46 (82.1%)	1A4M, 1B66, 1DES, 1HS6, 1HWW, 1HXR, 1ITK, 1IP33, 1IP6O, 1P33, 1TQO, 1UAQ, 1UWZ, 1UX0, 1UX1, 1Y13, 2A0S, 2ALW, 2DQDM, 2F18, 2F1B, 2F7Q, 2F7R, 2FR5, 2O3K, 3BKK, 3BLB, 3BUP, 3BUQ, 3BVW, 3BVX, 3CZS, 3D4Y, 3D4Z, 3D50, 3D51, 3DDF, 3DDG, 3DX0, 3DX1, 3DX2, 3DX3, 3DX4, 3EJP, 3EJQ, 3EJR, 3EJT, 3EJU, 3EWC, 3EWD, 3FX6, 3LGG, 3QNA
hydroxyl amide	0	3	3 (100.0%)	3 (100.0%)	1GW6, 2HPT, 2XQQ
imidazole	0	12	2 (16.7%)	6 (50.0%)	1C2E, 1C2K, 1XUG, 2JEW, 3IKF, 3PB7, 3PB8, 3PBB, 3PZ3, 3S12, 3E37
keto-carboxylic acid	-1	5	1 (20.0%)	2 (40.0%)	1SR9, 2YYF, 2Y7G, 3D8C, 3HPS
pyridine	0	3	1 (33.3%)	3 (100.0%)	3JVH, 3KE1, 3O94
sulfamate	-1	13	7 (53.8%)	12 (92.3%)	1EOU, 1ITM, 1XPZ, 2WD2, 3DD8, 3HKU, 3IBL, 3IBU, 3LXE, 3T82, 3T84, 3T85
sulfonamide	-1	44	26 (59.1%)	34 (77.3%)	1IF7, 1IF9, 1JD0, 1OKL, 1ZH9, 2EU2, 2H4N, 2NN7, 2Q1Q, 3B4F, 3BL0, 3CZV, 3DAZ, 3DBU, 3DCS, 3DCW, 3DD0, 3F7B, 3F7U, 3FFP, 3HKQ, 3HKT, 3K2F, 3M04, 3M2Y, 3M3X, 3MHC, 3ML5, 3QYK, 3RYV, 3RYY, 3RZ2, 3S72, 3S73, 3S75, 3S76, 3SAP
thiol	-1	11	7 (63.6%)	7 (63.6%)	1F57, 1J37, 1UZE, 1Y8J, 1ZG8, 2O10, 2OSM, 2X8Z, 3B92, 3C8Z
other ^c		18	9 (50.0%)	12 (66.7%)	1GI4, 1HDQ, 1HDU, 1HEE, 1IY7, 1LT8, 2DVX, 2GKL, 2QJB, 2RFH, 2Z94, 2ZA0, 3FOR, 3FVL, 3M1K, 3M2X, 2Q38, 3K14

^aSuccess rates of scoring with the FACTS solvation model are reported. ^bNumber of successful cases in classical and QM/MM scoring (percentage in parentheses) for each ZBF for which there are less than three cases.

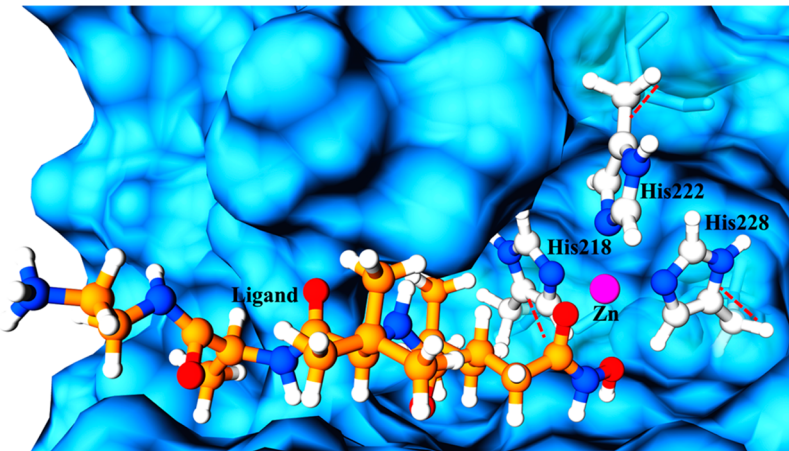


Figure 1. Example of a QM/MM setup (PDB ID 1BKC): The QM system is shown in ball and stick representation, the MM system in surface and stick representation, and the QM/MM boundaries are marked by red lines.

procedure yielded 226 complexes for the zinc-binding dataset and 55 complexes for the zinc-nonbinding dataset. There is no overlap between our test set and the smaller zinc metalloprotein test sets of 40 complexes⁴⁸ and 23 complexes,¹⁵ used in previous works. However, 4 complexes from our test set (PDB ID 1HWW, 1IY7, 1JD0, 1LRH) are present in the “highly trustworthy” subset of the iridium database,⁵⁶ and one is present in its “medium trustworthy” subset (1R55).

2.2. Setup of Ligand–Protein Complexes. For setup of the ligands, we extracted the respective coordinates from the Protein Databank (PDB) file, added hydrogen atoms using the “AddH” utility in UCSF CHIMERA (<http://www.cgl.ucsf.edu/chimera>),⁶¹ and carefully adjusted bond orders and protonation states by visual inspection. Protonation states were determined based on pK_a values and structural data for some cases, leading to the formal charges of the zinc-binding functionalities reported in Table 1. For example, hydroxamic acids were kept in their neutral form,⁶² while carboxylic acids were described in their anionic form.⁵³ Ligand force-field parameters were derived based on the Merck Molecular Force Field⁶³ using the SwissParam algorithm.⁵⁷

For setup of the protein–ligand complexes, we removed all water molecules and heteroatoms except for the ligand and monatomic ions. When nonperiodic images of the protein were present, all chains within a distance of 8 Å of the ligand were included in the model. The protein was modeled using the all-atom CHARMM22 force field,^{64–66} and the Zn ion was described by the nonbonded Stote/Karplus model, carrying a charge of +2.⁶⁷ Hydrogen atoms were added using the HBUILD procedure of CHARMM.³⁹ Protonation states of histidine and catalytic glutamate/aspartate side chains were chosen based on the environment. Complexes were optimized in CHARMM using 100 steps of steepest descent (SD). During optimization, the ligand and the Zn atoms were held fixed, while all other heavy atoms were restrained with a force constant of 5 kcal/mol/Å² to their original position.

2.3. Classical Docking. Classical docking was carried out with a 2-fold purpose: (i) to benchmark the QM/MM scoring function against the purely classical scoring function of our in-house docking algorithm EADock DSS,^{40,68,69} and (ii) to create an ensemble of 250 binding poses for each complex to be subject to QM/MM optimization and scoring. EADock DSS uses a dihedral space sampling (DSS) algorithm to generate relevant ligand conformations, which are ranked by two scoring

functions based on the CHARMM22^{64–66} force field. In brief, individual binding modes are evaluated by the fast and efficient SimpleFitness (SF_{MM}) as defined in eq 1.

$$SF_{MM} = E_{intra,lig} + E_{intra,prot} + E_{vdw} + E_{elec} \quad (1)$$

Here, $E_{intra,lig}$ and $E_{intra,prot}$ are the internal energies of ligand and protein, respectively. E_{vdw} and E_{elec} are the van der Waals and electrostatic interaction energies between the ligand and the protein. The classically minimized binding modes were clustered by root-mean-square deviation (RMSD) with a distance cutoff of 2 Å, and the maximal cluster size was set to 8. Clusters of binding modes are then evaluated by the more accurate but slower FullFitness (FF_{MM}), which takes solvation into account (eq 2).

$$FF_{MM} = SF_{MM} + \Delta G_{solv} \quad (2)$$

The solvation energy (ΔG_{solv}) is composed of an electrostatic contribution ($\Delta G_{elec,solv}$), calculated by an implicit solvent model, and a nonpolar contribution proportional to the solvent-accessible surface area (SASA) (see eq 3).

$$\Delta G_{solv} = \Delta G_{elec,solv} + (\sigma \times SASA) \quad (3)$$

Here, $\Delta G_{elec,solv}$ was computed using the “Fast Analytical Continuum Treatment of Solvation” (FACTS)⁷⁰ or the “Generalized Born Molecular Volume 2” (GBMV2)⁷¹ solvation models with a solute dielectric constant of 1. The surface tension coefficient (σ) was set to 0.0075 kcal/mol/Å² in combination with FACTS and to 0.0072 kcal/mol/Å² in combination with GBMV2.

In order to create ensembles of 250 binding poses for each complex, we performed local dockings in a cubic box with an edge length of 20 Å. For zinc binders, the box was centered at the center of mass of the X-ray pose of the ligand, whereas for zinc nonbinders, the box was centered at the geometric center between the Zn ion and the center of mass of the X-ray pose of the ligand to allow for spurious zinc binding. The number of generated binding modes was set to 30 000, and the ligand was minimized by 100 steps of SD followed by 1000 steps of adopted basis Newton–Raphson (ABNR) algorithm. The optimized X-ray pose (50 steps of SD and 50 steps of ABNR) was added to the binding pose ensembles to eliminate the influence of sampling failures upon the scoring assessment.

2.4. QM/MM Docking. For each complex, the ensemble of 250 docking poses generated by EADock DSS, as well as the

optimized X-ray structure, were subject to optimization and rescoring with the SCC-DFTB QM/MM scheme²¹ in CHARMM³⁹ (version 36b1). SCC-DFTB parameters for zinc, carbon, nitrogen, oxygen, sulfur, and hydrogen (the “znorg” set)⁶⁰ were downloaded from www.dftb.org. The Zn ion, its coordinating protein side chains, and the ligand were included in the QM part, while the remainder of the system was treated at classical molecular mechanics (MM) level and kept fixed (Figure 1). We also defined a “SmallQM” model, in which only the Zn ion and the ligand were included in the QM system. Valencies at the QM/MM interface were satisfied by hydrogen link atoms, which were harmonically restrained to their initial position, using a force constant of 0.2 kcal/mol/Å². The QM atoms interact with the MM atoms through electrostatic and van der Waals terms. To achieve convergence of the SCC-DFTB calculations, the electronic temperature was set to 300 K. Geometry optimization was performed with 900 steps of SD and 100 steps of ABNR algorithm to avoid convergence problems and to keep the diversity among the ensemble of 250 binding poses, leading to an average root-mean-square gradient of 0.2 kcal/mol/Å for successful poses. Different contexts, such as the treatment of different metalloproteins or larger ligands, might require an adaptation of the optimization scheme.

In analogy to its classical counterpart, the QM/MM FullFitness was defined as

$$\text{FF}_{\text{QM/MM}} = E_{\text{QM/MM}} + \Delta G_{\text{solv}} \quad (4)$$

Here, $E_{\text{QM/MM}}$ (QM/MM Simple Fitness) is the total energy of the complex in the QM/MM scheme. The solvation term was calculated with the FACTS solvation model on the optimized binding pose as in the classical scoring function, but using Mulliken charges for the atoms belonging to the QM region.

If during optimization any bond of the ligand not involving a hydrogen atom increased its length to more than 0.5 Å above its optimal classical bond length value, the bond was considered broken and the pose was omitted from further analysis.

2.5. Classical Docking with AutoDock4 and AutoDock Vina. We compared the performance of our docking approaches with the widely used docking programs AutoDock4^{72,73} and AutoDock Vina,⁷⁴ as well as the recently improved AutoDock4 force field for zinc metalloproteins (AutoDock4Zn).⁵¹ AutoDock Tools scripts with default settings were used to convert the PDB files of the receptors and the MOL2 files of the ligands into PDBQT format. The center of the cubic search space with an edge length of 20 Å was defined as for EADock DSS. Zn ions were assigned a charge of +2, except in the case of AutoDock4Zn, where zinc does not carry a charge. In AutoDock4Zn, TZ pseudoatoms were added with a Python script available from the authors.

In AutoDock4, the grid point spacing was set to 0.375 Å. Docking was performed with 200 independent runs of the Lamarckian Genetic Algorithm,⁷⁵ using a maximum of 25×10^6 energy evaluations, a maximum number of 27×10^3 generations, a gene mutation rate of 0.02, and a crossover rate of 0.8. For AutoDock Vina,⁷⁴ the exhaustiveness was set to 500 (default 8), and the maximum number of binding modes in the output was set to 20 (default 9).

2.6. Data Analysis. The docking poses were ranked according to their FullFitness. If the pose with the most favorable FullFitness had a RMSD below 2 Å with respect to the X-ray pose, a success was reported. Ligand symmetry was taken into account for RMSD calculation.

For the zinc-binding dataset, we calculated the distances between the Zn ion and all ligand atoms in the X-ray structure. If only one ligand atom displayed a Zn distance of <2.5 Å, monodentate zinc binding was assumed. If two ligand atoms displayed a Zn distance of <2.5 Å, bidentate zinc binding was assumed. During analysis of the docking results, correct zinc binding was reported if one (monodentate) or both (bidentate) original zinc-binding atom(s) of the best predicted docking pose displayed a Zn distance of <2.5 Å. Because of steric constraints, we found that correct zinc binding was generally equivalent to a correct coordination geometry.

In order to investigate the capabilities of different approaches to detect correct tetrahedral zinc coordination geometries, we followed the definitions developed in the AutoDock4Zn approach.⁵¹ Briefly, for Zn atoms coordinated by three protein atoms and one ligand atom (123 complexes of the zinc-binding dataset), a plane was defined as being composed of the three receptor atoms. The deviation from an ideal tetrahedral geometry was calculated as the angle between the normal of this plane and the Zn–ligand atom vector (TAng). If, in the X-ray structure, TAng < 20°, a tetrahedral complex was defined (95 complexes). For zinc-coordinating Asp and Glu side chains, a weighted average position for the two carboxylate oxygens was calculated and they were considered as monodentate ligands, according to Santos-Martins et al.⁵¹

For both datasets, we also calculated the minimal distance between the Zn ion and all ligand atoms in the highest ranked docking pose. If this distance was <2.5 Å, a zinc-bound conformation was reported. In addition, we investigated the influence of the fraction of the surface of the ligand that was buried upon complexation in the X-ray structure (Lig-BS). The higher this value, the smaller the surface of the ligand accessible to bulk solvent.

2.7. Calculation of Hydration Free Energies. In order to test the performance of the FACTS solvation model with the standard SwissParam small-molecule force fields⁵⁷ and in combination with the QM/MM-derived Mulliken charges, we used the FreeSolv database of experimental hydration free energies of 643 small molecules;⁷⁶ 459 of these compounds can be treated with the employed SCC-DFTB parameters for elemental carbon, nitrogen, oxygen, sulfur, and hydrogen.⁶⁰ For each of these compounds, we derived force-field parameters using the SwissParam algorithm and generated a maximum of 20 conformations with the excalc program from Chem3D Pro. Each conformation was optimized in CHARMM using 250 steps of SD with a gradient tolerance of 0.1 kcal/mol/Å, and its solvation free energy was calculated with FACTS using the same parameters as during the docking calculations. A Boltzmann averaging over all conformations yielded ΔG_{solv} for each compound.

3. RESULTS AND DISCUSSION

In this work, we developed a SCC-DFTB/CHARMM QM/MM scoring function for the docking algorithm EADock DSS and tested its application to zinc metalloproteins. We carefully devised a dataset limited to druglike ligands and high-quality X-ray structures, characterized by a low DPI and complete and unambiguous ligand coordinates. We considered not only complexes where the ligand is directly coordinated to the Zn ion (zinc-binding dataset), but also complexes where the ligand is not in direct contact with the metal ion, although a free coordination site exists (zinc-nonbinding or allosteric dataset). This second dataset yields crucial information, because a

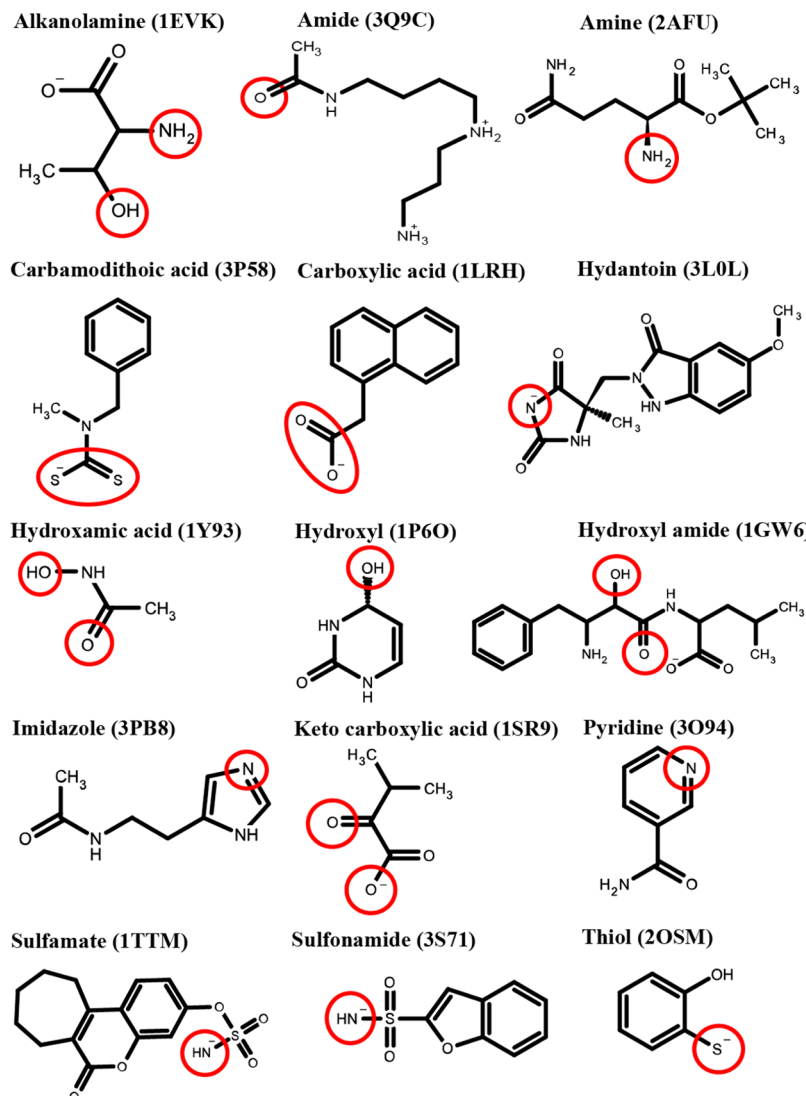


Figure 2. Examples of zinc-binding functionalities, with metal-binding atoms marked in red.

scoring function could perform well for the first by over-emphasizing the ligand–Zn binding energy, with respect to other terms. It is also informative for virtual screening studies, where zinc binders need to be distinguished from nonbinders. For each complex of the test sets, we created an ensemble of 250 ligand poses by classical docking with EADock DSS, which was then rescored with different solvation models and scoring functions. Since we are interested in scoring rather than sampling, we also included the minimized X-ray pose in the ensembles.

3.1. Datasets. Although our dataset was compiled purely based on structural criteria, it covers a large number of different enzymes (41 in the binding dataset, 15 in the nonbinding dataset) from all six enzyme classes (see Tables S2 and S3 in the Supporting Information) and features many interesting drug targets. These include the following examples: ADAM17 endopeptidase, also known as TNF- α converting enzyme (TACE), which has been associated with the development of several diseases;^{77–81} alpha-mannosidase II, which is an anticancer target;⁸² carbonic anhydrases, which are a target for antiglaucoma and anticancer therapy;^{83,84} and MECDP synthase, which is a potential target for antimicrobial therapy.^{85,86} Many enzymes (for example, MECDP synthase,

adenosine deaminase, carbonic anhydrase, carboxypeptidase, and thermolysin) are present both in the zinc-binding dataset and the zinc-nonbinding dataset, allowing for a direct comparison of the scoring results for competitive and allosteric ligands. One X-ray structure (PDB ID: 2AFU) is simultaneously present in both datasets, because its ligand binds to two different sites in the asymmetric units. The presence of multiple structures of some proteins in complex with different ligands provides the opportunity to carry out cross-docking studies, although this is beyond the scope of the present work.

The ligands from the zinc-binding dataset show a large range of different zinc-binding functionalities (see Table 1, as well as Figure 2), featuring neutral and negatively charged zinc-binding groups, and showing monodentate (64.6% of test cases) or bidentate (35.4%) zinc binding. Most bidentate ligands coordinate to zinc through a vicinal diol or a hydroxamic acid moiety. The most prevalent zinc-binding atom is oxygen (64.4%), followed by nitrogen (29.7%) and sulfur (5.9%). Many ligands are known drugs or druglike molecules of the hydroxamic acid, sulfonamide, or sulfamate type. The properties of the two test sets are very similar, in terms of the size of the ligands, their number of rotatable dihedrals, the number of resolved ligand-bound water molecules in the X-ray structure,

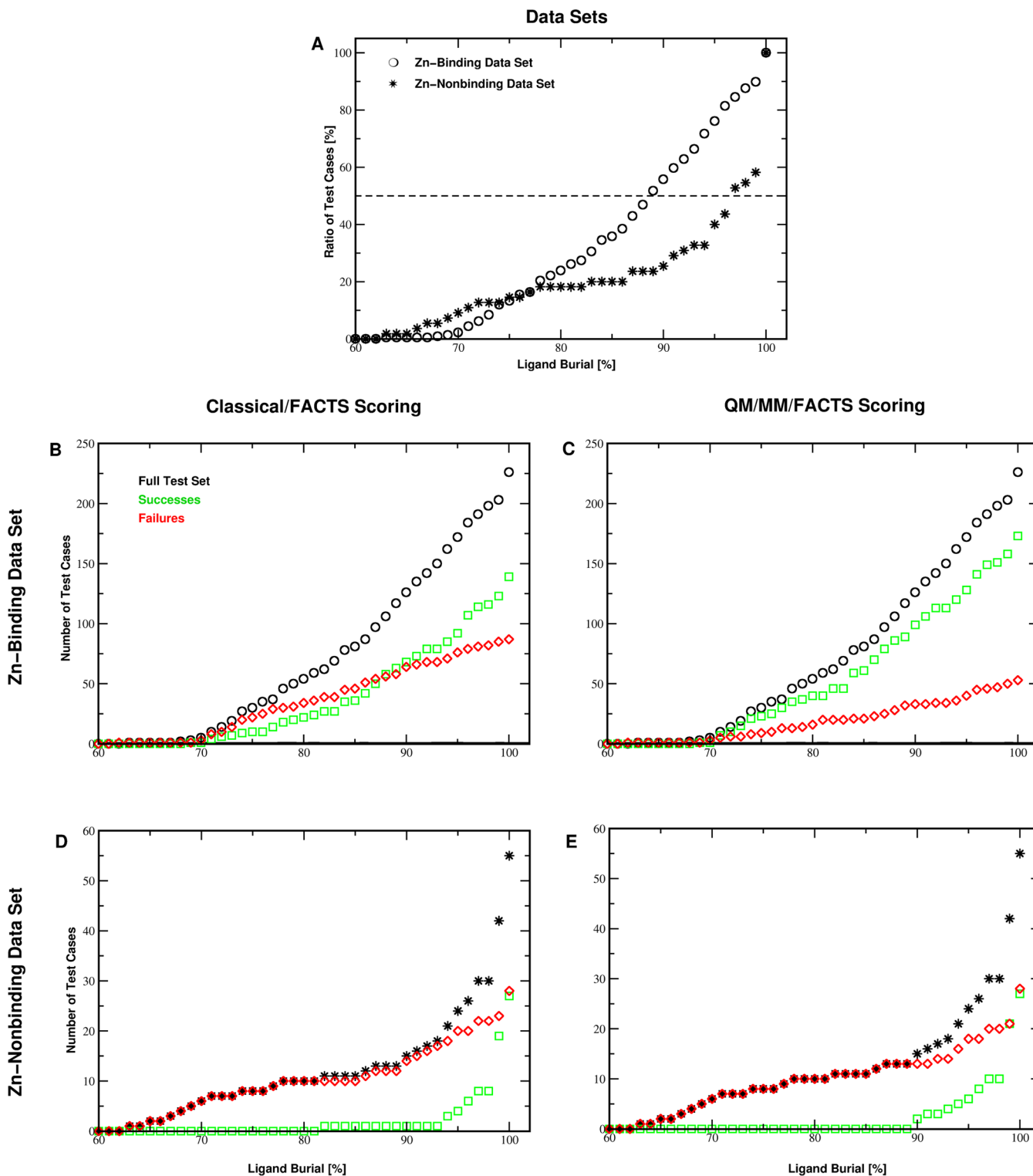


Figure 3. (A) Cumulative histograms of the ligand burial in the X-ray structures of the zinc-binding (circles) and of the zinc-nonbinding (stars) datasets. (B–E) Cumulative histograms of the successes (green) and failures (red) of the classical/FACTS (panels B and D) and the QM/MM/FACTS (panels C and E) scoring schemes for the zinc-binding dataset (panels B and C) and for the zinc-nonbinding dataset (panels D and E).

and the burial of the Zn ion (for details, see Table S1 in the Supporting Information). In the nonbinding dataset, there generally is one water molecule bound to the Zn ion, and the average ligand–Zn separation amounts to 4.8 Å. Although the average burial of the protein-bound ligands (Lig-BS) is similar between the two test sets, their distributions differ significantly. The binding set features an approximately homogeneous

distribution between 70% and 100%, whereas, in the nonbinding set, 45% of ligands are buried more than 99% and 11% are very solvent exposed (Lig-BS < 70%; see Figure 3A).

These manually curated high-quality protein–ligand complexes are available at <http://www.molecular-modelling.ch/resources.php> in a format ready to be used for docking and

Table 2. Success Rates (Ligand RMSD < 2 Å in Highest Ranked Docking Pose) for All Scoring Schemes and Docking Algorithms

scoring scheme	Zinc-Binding Dataset (226 Complexes)		Zinc-Nonbinding Dataset (55 Complexes)	
	excluding X-ray pose	including X-ray pose	excluding X-ray pose	including X-ray pose
classical/vacuo	139 (61.5%)	157 (69.5%)	20 (36.4%)	21 (38.2%)
classical/GBMV2	43 (19.0%)	48 (21.2%)	22 (40.0%)	22 (40.0%)
classical/FACTS	137 (60.6%)	139 (61.5%)	26 (47.3%)	27 (49.1%)
AutoDock4	68 (30.1%)		10 (18.2%)	
AutoDock4Zn	98 (43.4%)		21 (38.2%)	
AutoDock Vina	130 (57.5%)		31 (56.4%)	
QM/MM/vacuo	125 (55.3%)	141 (62.4%)	13 (23.6%)	14 (25.5%)
QM/MM/FACTS (small QM)	144 (63.7%)	168 (74.3%)	14 (25.5%)	15 (27.3%)
QM/MM/FACTS SPE	145 (64.1%)	175 (77.4%)	26 (47.3%)	28 (50.9%)
QM/MM/FACTS	148 (65.5%)	174 (77.0%)	23 (41.8%)	27 (49.1%)

cross docking using the SwissDock web server⁶⁸ (<http://www.swissdock.ch/>).

3.2. Generation of Binding Mode Ensembles and Classical Docking.

In order to create an ensemble of 250 ligand poses for each complex, we carried out classical local docking calculations using our in-house docking program EADock DSS⁴⁰ with enhanced sampling parameters to minimize sampling failures. In 92.5% of the zinc-binding test cases and in 87.3% of the zinc-nonbinding test cases, the generated ensemble included a successful pose reproducing the native pose with a RMSD below 2 Å. To ensure that a rescoring approach can possibly detect a successful binding pose also for the remaining cases, we included the minimized X-ray pose in the ensembles.

The classical scoring function⁶⁹ of EADock DSS is based on the CHARMM22^{64–66} all-atom force field, which includes the nonbonded zinc model developed by Stote and Karplus⁶⁷ that has been developed and validated for the use with an explicit solvent description. In earlier docking studies, it was found that the use of this zinc model, in combination with the GBMV2⁷¹ implicit solvent model, yielded a very low success rate for zinc metalloproteins (33%).⁵⁰ Here, we rescored the ensembles of docking poses generated by EADock DSS without solvation as well as with the GBMV2 and with the FACTS⁷⁰ implicit solvation models (see Table 2).

For the zinc-binding dataset, we obtained a high success rate with the classical scoring neglecting solvation effects (69.5%, Table 2). This success rate decreased drastically upon addition of solvation with the GBMV2 model (21.2%), and to a lesser extent also with the FACTS model (61.5%). Analysis of the data shows that the solvation models drive the ligands away from the highly charged Zn ion, because of its very favorable solvation energy, thus decreasing the success rate (Figure 4A). However, it should be kept in mind that, generally, it is crucial for scoring functions to account for solvation effects.⁶⁹

This is also evident from the results for the allosteric dataset, where the highest success rate (49.1%; see Table 2) was obtained with the FACTS model. Without solvation the success rate was substantially lower (38.2%). The generally lower success for the allosteric test set, when compared to the zinc-binding set, can partially be attributed to spurious zinc binding. With FACTS solvation, in 27.3% of the cases, the best predicted binding mode erroneously binds to the Zn ion (see Table S4 in the Supporting Information and Figure 4B). It should be noted that, in 94.5% of the X-ray structures from the nonbinding dataset, a zinc-bound water molecule was removed during setup. A smart treatment of active site solvation such as

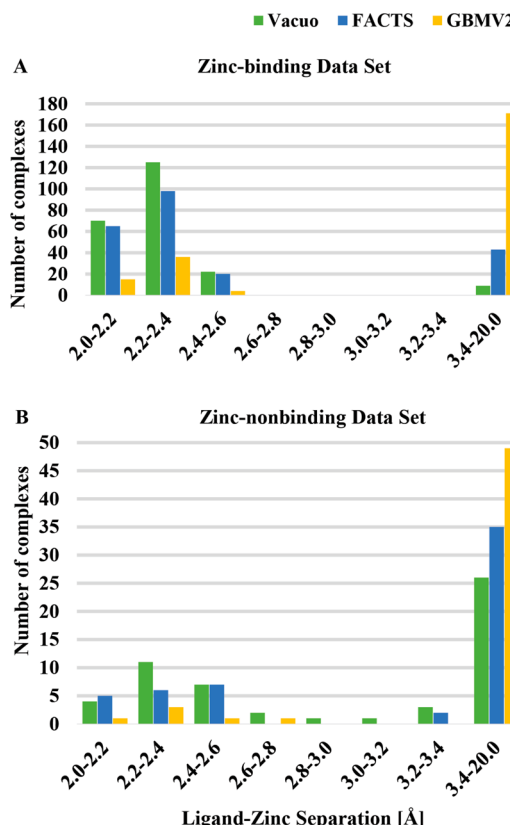


Figure 4. Classical scoring schemes: effect of solvation models upon ligand–Zn separation in highest ranked docking pose for (A) zinc-binding dataset and (B) zinc-nonbinding dataset.

WaterMap⁸⁷ may be able to avoid overbinding. A further decrease in the success rate is due to limited protein–ligand contacts in some complexes. All ligands with more than 20% of their surface exposed to the bulk solvent (18.2% of the test cases) could not be ranked correctly, independent of the solvation model (Figure 3D). Similar trends were observed previously for a different dataset.⁴⁰

For the zinc-binding dataset, in addition to the RMSD-based docking assessment, we also investigated the zinc-binding geometries of the best predicted docking poses. First, we determined if the scoring functions were able to identify the correct zinc-binding atom(s). This observable is complementary to the ligand RMSD, because in many ligands (e.g., sulfonamides or sulfonamides), it is conceivable that a ligand pose

Table 3. Determination of Correct Zinc-Binding Atom(s) in Best Docking Pose of the Zinc-Binding Dataset^a

scoring scheme	Excluding X-ray Pose			Including X-ray Pose		
	Mono	Bi	total	Mono	Bi	total
classical/vacuo	66	49	115 (50.9%)	73	60	133 (58.8%)
classical/GBMV2	21	18	39 (17.3%)	23	22	45 (19.9%)
classical/FACTS	61	37	98 (43.4%)	65	41	106 (46.9%)
AutoDock4	34	20	54 (23.9%)			
AutoDock4Zn	92	25	117 (51.8%)			
AutoDock Vina	58	37	95 (42.0%)			
QM/MM/vacuo	113	56	169 (74.8%)	118	64	182 (80.5%)
QM/MM/FACTS (small QM)	124	65	189 (83.6%)	127	73	200 (88.5%)
QM/MM/FACTS SPE	108	53	161 (71.2%)	121	64	185 (81.9%)
QM/MM/FACTS	114	59	173 (76.5%)	121	68	189 (83.6%)

^aThe set consists of 146 monodentate (Mono) and 80 bidentate (Bi) Zn–ligand complexes.

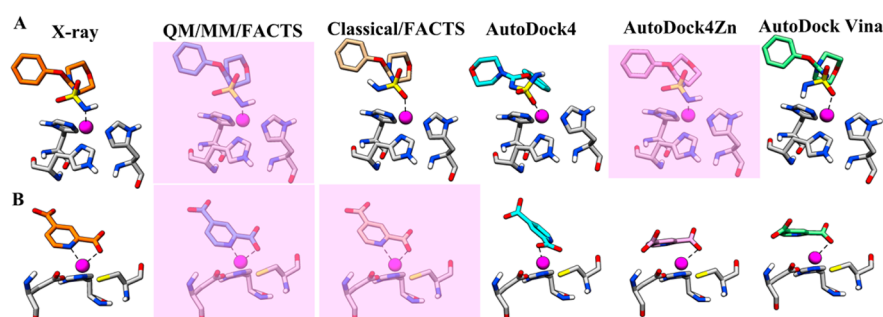


Figure 5. Prediction of zinc-binding geometries by different docking/scoring algorithms: (A) typical sulfonamide binding to zinc (PDB ID 3M04) and (B) typical bidentate ligand binding to zinc (PDB ID 2GKL). Correctly predicted zinc-binding geometries are highlighted in pink.

with a RMSD of <2 Å shows zinc binding through an incorrect atom. On the other hand, it is possible that a docking pose shows correct zinc binding but an overall RMSD above 2 Å. As shown in Table 3, the classical scoring schemes without solvation (58.8%) and with FACTS solvation (46.9%) were less successful at correctly predicting the details of the zinc-binding motifs than they were at predicting the overall RMSD of the ligands. In the case of GBMV2, the success rate remained equally low (19.9%). Closer examination showed that the main problem in the classical scoring schemes is that most sulfamates and sulfonamides were predicted to bind to Zn through an O atom instead of the N atom (see Figure 5A). We also investigated if the geometries of the 95 tetrahedral complexes were reproduced with a deviation of <20° from an optimal tetrahedral angle. Here, the three classical scores perform badly, correctly reproducing tetrahedral geometries only in 10.5%–21.1% of the test cases (see Table S5 in the Supporting Information). Again, bad results are mostly due to oxygen-bound sulfamates and sulfonamides, which account for 58.9% of the tetrahedral complexes.

Taken together, the results from classical scoring functions suggest that they yield better results for buried ligands than for solvent-accessible ligands. The vacuo results favor direct ligand–Zn interactions; therefore, greater success is obtained for the zinc-binding dataset than for the nonbinding dataset. On the other hand, the GBMV2 model drives the ligand away from the Zn ion because it strongly favors a solvated Zn ion. The FACTS model seems to provide the best balance between these two opposite effects and yields very good success rates for both test sets. Since it has the additional advantage of being computationally less demanding than GBMV2, we used this model in the following for the QM/MM score.

3.3. Comparison of Classical Docking Codes. In order to compare the results of EADock DSS with widely used open-source docking programs, we also applied AutoDock Vina⁷⁴ and AutoDock4,^{72,73} both with its standard force field as well as with its specially parametrized AutoDock4Zn force field,⁵¹ to the two test sets. AutoDock Vina formally treats metals as hydrogen-bond donors. In AutoDock4, ligand–Zn interactions are described through van der Waals and electrostatic terms, similar to their treatment in CHARMM. In AutoDock4Zn, the Zn ion has a zero charge, switching off electrostatic interaction terms. The van der Waals term was tuned to reproduce experimentally observed zinc-binding distances, and a new directional potential was added to improve tetrahedral geometries. On their test set of 292 zinc metalloprotein complexes, the authors found that the new scoring function led to an improved success rate (45%) over standard AutoDock4 (36%).

To achieve a fair comparison between these classical docking algorithms, we applied strongly enhanced sampling parameters in all cases (see Section 2.5) and compared the success rates to the EADock DSS success rates obtained on the original docking ensembles without the X-ray pose (Table 2). For the zinc-binding dataset, the classical EADock DSS/FACTS model (success rate 60.6%) outperformed AutoDock4 (30.1%), AutoDock4Zn (43.4%), and AutoDock Vina (57.5%). AutoDock4 (23.9%) also yielded a lower rate of correctly predicted zinc-binding motifs (43.4% for Classical/FACTS, Table 3), while AutoDock Vina yielded comparable results (42.0%). AutoDock4Zn predicted monodentate Zn–ligand complexes well but did not improve the description of bidentate complexes, resulting in a rate of 51.8% of correctly predicted zinc-binding motifs (see Table 3). Regarding

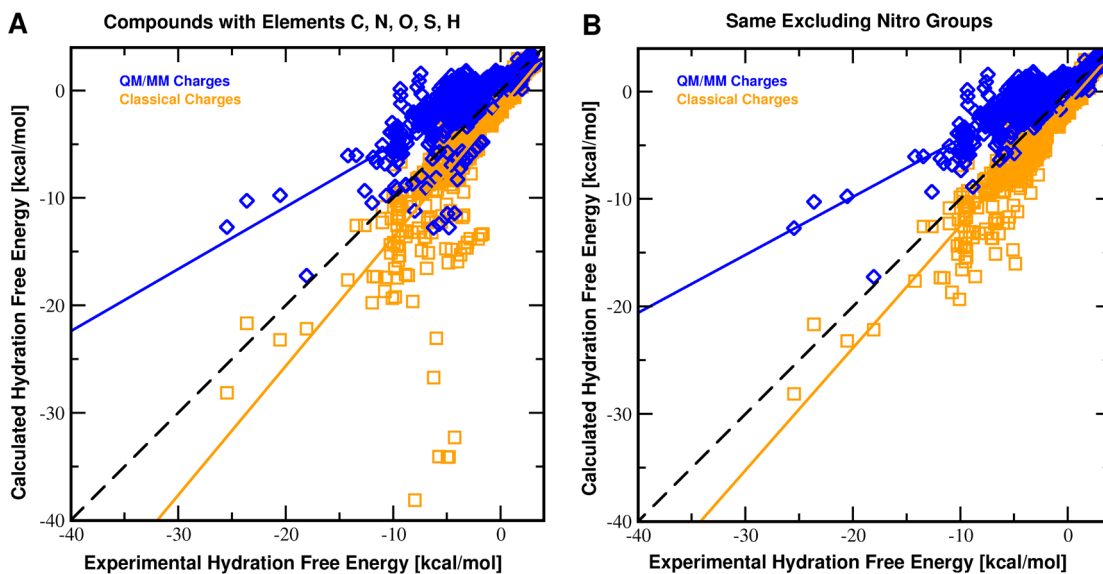


Figure 6. Correlation between experimental and calculated hydration free energies for the FreeSolv database using the FACTS solvation model with the classical SwissParam charges (orange) and with the SCC-DFTB-derived Mulliken charges (blue).

tetrahedral coordination geometries, the specially parametrized AutoDock4Zn force field largely outperformed all other classical docking schemes with 78.9% of correct geometries versus only 10%–20% for the other schemes (see Table S5 in the Supporting Information). A large part of the improvement of the AutoDock4Zn force field is due to the reduction of oxygen-bound sulfamates and sulfonamides among the best predicted docking poses (see Figure 5A).

For the zinc-nonbinding dataset, AutoDock Vina yielded the highest success rate (56.4%) compared to EADock DSS/FACTS (47.3%), AutoDock4Zn (38.2%), and AutoDock4 (18.2%; recall Table 2). Detailed analysis showed that both AutoDock4 and AutoDock Vina failed for very solvent-accessible ligands, similar to EADock DSS. However, AutoDock Vina does not suffer from overbinding (observed only in 7.3% of cases, Table S4 in the Supporting Information) and, therefore, yields a good success rate for the nonbinding dataset.

In summary, the performance of EADock DSS/FACTS on the zinc-binding dataset compares favorably to the AutoDock approaches. This is an interesting result, because this scoring is employed in the freely available SwissDock web service (www.swissdock.ch).⁶⁸ AutoDock4Zn improves the description of monodentate zinc-ligating geometries but still yields a lower success rate for the overall reproduction of native ligand poses.

3.4. QM/MM Scoring. To comprehensively describe the charge-transfer effects in the active site of zinc metalloproteins, we included the Zn ion as well as the Zn–ligating protein side chains and the small organic ligands in the QM subsystem. An example of the employed QM/MM partition is given in Figure 1. To allow for structural relaxation with the QM/MM scoring function, we optimized the QM subsystem of all classically obtained poses within the QM/MM scheme, keeping the classically described surrounding fixed. Contrary to a classical force field, the molecular topology of a ligand is not predefined in a quantum chemical description and therefore can change during geometry optimization. This is occasionally observed in our approach, but mostly when starting the optimization from strained ligand conformations in less-favorable binding poses. Exclusion of these “broken” ligand conformations from further analysis did not change the calculated success rates. Only in one

case (PDB ID 3KGQ) the best predicted binding pose consisted of a broken conformation, i.e., the citric acid ligand eliminated CO₂ to form acetonedicarboxylic acid (see Figure S1A in the Supporting Information). Since the FACTS solvation model provides the most balanced description of electrostatic desolvation in the classical docking, it was used for the QM/MM scoring function.

For the zinc-binding dataset, the QM/MM scoring function with the FACTS solvation model yielded a very high success rate (77.0%; recall Table 2), a significant improvement compared to the success rate of 61.5% obtained with the classical/FACTS score. At the same time, the success rate for the nonbinding dataset remained constant (49.1%; see Table 2). Zn–ligand binding is more favorable in the QM/MM scheme, as demonstrated by the increased ratio of zinc-bound ligand poses among the best-predicted binding poses (see Table S4 in the Supporting Information). In the zinc-binding set, 92.5% of the top poses display zinc binding (classically, 79.2%), and in the allosteric test set, 47.3% of the top poses display zinc binding (classically, 27.3%). Overbinding thus accounts for most of the failures in the nonbinding dataset, followed by the inability to predict native binding modes of ligands with a buried surface area of <80% (see Figure 3E). In the zinc-binding dataset, since there is a strongly favorable ligand–Zn interaction, the dependence on ligand burial is weaker (see Figure 3C).

The QM/MM scheme describes the interactions between the ligand, the Zn ion, and its coordinating protein side chains on a higher level than the classical force field, taking into account quantum effects and the transfer of electronic density between these entities. The average Mulliken charge on the Zn ion in the zinc-binding dataset amounts to +0.4 ± 0.1, which is significantly reduced from its formal charge of +2 in the classical force field. Most of this charge (+1.2 ± 0.1) is redistributed to the coordinating protein side chains, while a smaller part is transferred to the ligand (+0.4 ± 0.2). In addition to a good estimation of the Zn–ligand binding energy, the reduced charge on the Zn ion leads to a reduced electrostatic solvation energy and, therefore, favors zinc-bound ligand poses.

In order to test the performance of the FACTS solvation model with the standard SwissParam small-molecule force fields⁵⁷ and in combination with the QM/MM-derived Mulliken charges, we used the FreeSolv database of experimental hydration free energies of 643 small molecules;⁷⁶ 459 of these compounds can be treated with the employed SCC-DFTB parameters for carbon, nitrogen, oxygen, sulfur, and hydrogen.⁶⁰ As it can be appreciated from Figure 6, the hydration energy of nitro groups is strongly overestimated in the classical force field and, to a lesser extent, also with the Mulliken charges. Interestingly, during docking, out of 4 complexes with ligands featuring nitro groups, 3 led to failures in all scoring schemes. Removal of the 29 nitro compounds from the hydration test set led to a R^2 value of 0.85 for the classical charges (root mean square error (RMSE) = 1.84 kcal/mol) and of 0.69 for the QM/MM charges (RMSE = 1.38 kcal/mol) (see Figure 6B). The slope (1.14) is closer to unity for the classical charges than for the generally lower Mulliken charges (0.54), which implies that ligand solvation energies are underestimated in our docking approach. A more elaborate implicit solvation model developed especially for SCC-DFTB⁸⁸ may be tested in future studies.

The QM/MM/FACTS scoring function showed a very good performance for the detection of correct zinc-binding motifs (83.6%; recall Table 3), substantially improved over the classical/FACTS scoring (46.9%). The improvement of zinc-binding geometries is even more evident from the data for the 95 tetrahedral complexes, where a correct description increases from 15.8% to 85.3% (see Table S5 in the Supporting Information). Closer investigation showed that most of the improvement in the QM/MM approach is due to (i) the correct nitrogen-bound pose prediction for sulfamates and sulfonamides among the monodentate ligands (Figure 5A), and (ii) the correct bidentate pose prediction (Figure 5B), especially for hydroxamic acid and vicinal diol ligands. These improvements demonstrate the value of the QM/MM approach when describing the details of ligand–metal binding.

In order to mimic a rescoring docking approach, where only the results of a classical docking are treated by the QM/MM score, we also calculated the success rates for the ensembles without the X-ray structure (recall Table 2). As expected, for the classical scoring with FACTS, this does not significantly change the results (60.6% vs 61.5%), since, because of the enhanced sampling parameters and the limited number of rotatable ligand dihedrals, the failures are likely to be due to scoring deficiencies rather than sampling deficiencies. However, for the QM/MM scoring, the success rate decreases significantly (65.5% vs 77.0%), because now, in some cases, even though the QM/MM score could correctly identify the native pose, there is no sufficiently close pose present in the ensembles. This underlines that an on-the-fly docking approach would lead to better results than a rescoring of the final classical docking poses, since it would potentially identify the correct binding mode at an earlier stage and prevent its elimination by the deficient classical scoring. On the other hand, it is encouraging that, also under pure rescoring conditions, the QM/MM scoring function still yields an improvement over the classical scoring function.

A comparison between the success rates of the QM/MM/FACTS score and the classical scores of AutoDock4, AutoDock4Zn, and AutoDock Vina demonstrated that our hybrid scoring function outperforms these classical docking approaches for the zinc-binding dataset (see Table 2). For the

nonbinding dataset, AutoDock Vina showed the best results, because of its relatively weak zinc affinity. Regarding zinc-binding geometries (Table 3) and tetrahedral geometries (see Table S5 in the Supporting Information), the QM/MM/FACTS score also performed better than the three classical scores, including the specially parametrized AutoDock4Zn force field. Figure 7 shows a typical example, where the QM/

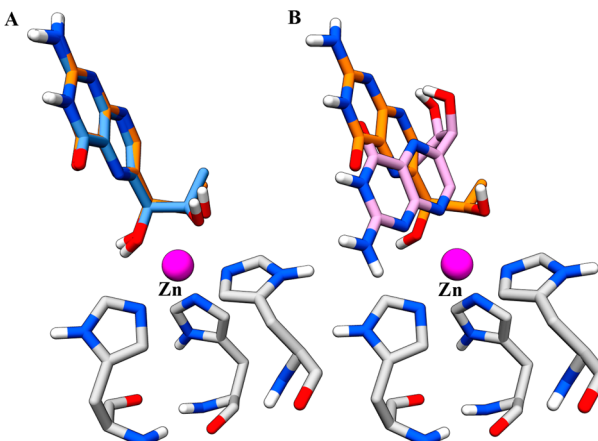


Figure 7. Comparison of QM/MM/FACTS score and AutoDock4Zn for a typical vicinal diol ligand (PDB ID 1Y13, ligand shown in orange). The best docking pose predicted by the QM/MM/FACTS score (panel A) shows a correct zinc-binding geometry and a good agreement with the native pose (RMSD 0.4 Å), while the best pose predicted by AutoDock4Zn (panel B) binds to zinc through a wrong atom and shows a higher RMSD value (4.2 Å).

MM scoring correctly reproduces the bidentate zinc binding of a vicinal diol, while AutoDock4Zn predicts the ligand to bind to Zn in a tetrahedral geometry through a single N atom.

The results for two enzyme families for which the differences between classical and QM/MM scoring were particularly significant—ADAM17 and carbonic anhydrases (Tables S2 and S3 in the Supporting Information)—will be further discussed in Sections 3.6 and 3.7.

3.5. Robustness of the QM/MM Scoring. To investigate the robustness of the QM/MM scoring function, with respect to different parameters, we performed additional calculations.

As a first test, we removed the FACTS solvation model from the scoring function, using the total QM/MM energy of the complexes as a score. This results in greatly reduced success rates both for the zinc-binding dataset (62.4% vs 77.0%; see Table 2) and for the nonbinding dataset (25.5% vs 49.1%), demonstrating that the solvation model is an important part of the scoring function, despite the underestimation of absolute ligand hydration free energies, as discussed above. Solvation has been found to be also important in classical ligand–protein docking.⁶⁹ However, this varies from the classical results for zinc-binding complexes, where the very favorable solvation energy of the Zn ion leads to a lower success rate when the FACTS solvation model is included in the score.

The influence of the size of the chosen QM region was tested by an alternative model (“small QM”), where only the ligand and the Zn ion were treated quantum mechanically, while the coordinating protein side chains were treated classically, prohibiting charge transfer between the protein and the Zn ion. During QM/MM minimization, many convergence failures occurred; however, in all test cases, at least one pose with an RMSD value of <2 Å, relative to the native pose, converged and

could be scored. Limitation of the charge transfer in this model is evident from the average zinc charge, which amounts to $+1.6 \pm 0.3$, instead of $+0.4 \pm 0.1$ in the standard QM/MM model. Here, the best ligand pose of 95.6% of the cases from the zinc-binding dataset and of 74.5% from the zinc-nonbinding dataset is in a zinc-bound conformation, demonstrating that zinc binding is strongly overemphasized. This is reflected in the success rate (recall Table 2), which remained almost constant for the zinc-binding dataset (74.3% vs 77.0%) but decreased significantly for the zinc-nonbinding dataset (27.3% vs 49.1%). These results again emphasize the importance of the allosteric dataset when benchmarking docking to metalloproteins.

As a final test, we investigated the effect of the QM/MM minimization by calculating the score directly on the classically generated binding poses (single point energy (SPE) calculations; see Table 2). Surprisingly, this performs as well as using the energies of the geometry optimized poses and barely changes the success rates. In 74.3% of all cases, the result remained the same, although in only 40.7%, the best pose remained the same. This demonstrates the details of the scoring change, but, generally, the same cluster of binding modes is ranked the highest, independent of the geometry optimization. This provides an advantage for on-the-fly docking, as computational time is greatly reduced for SPE calculations (see Table 4). However, it is not evident that single-point

Table 4. Median CPU Time Per Test Case Required for Docking/Scoring Using Different Approaches

docking approach	median CPU time [h]
classical/FACTS ^a	0.1
classical/GBMV2 ^a	0.3
AutoDock 4 ^b	11.0
AutoDock 4Zn ^b	11.4
AutoDock Vina ^b	1.0
QM/MM/FACTS (small QM) ^c	5.2
QM/MM/FACTS ^c	20.4
QM/MM/FACTS SPE ^a	0.3

^aCPU time required for rescoring without minimization (single point energy (SPE) calculation). ^bCPU time required for complete docking.

^cCPU time required for extensive QM/MM minimization and rescoring. All calculations were performed on Intel Xeon 2.83 GHz processors.

calculations will perform as well as geometry optimizations for different metalloproteins. In cases where ligand–protein interactions are less well-described by the classical score, as is the case, for example, for the interactions of covalent nature in hemoproteins, a stronger influence of the applied minimization scheme can be expected.⁴ In addition, omitting geometry optimization completely leads to significantly worse predicted tetrahedral zinc-binding geometries (see Table S5 in the Supporting Information), although this approach still outperforms the classical scores.

3.6. ADAM17 Results. With the QM/MM score, we obtained a success rate of 93.3% on the 15 ADAM17 complexes present in the zinc-binding dataset (see Table S2 in the Supporting Information), while the classical scoring function completely failed to correctly rank any of these complexes (0%). The fact that the classical score without solvation correctly ranked 73.3% of the cases, and the fact that all of the best poses predicted with the FACTS solvation model are far away from the Zn ion (>4.9 Å), suggest that FACTS pushes all ligands away from the active site, because of its very favorable solvation energy. This problem could be more severe for matrix metalloproteinases than for other enzymes because of the presence of a solvent-accessible polar glutamate in the active site.

Most of the ligands of ADAM17 (10/15) bind with a neutral hydroxamic acid functionality to the Zn ion, while the remainder bind either with a negatively charged hydantoin functionality (3 cases) or thiolate functionality (2 cases). Quantum mechanical studies on hydroxamic acid ligands binding to ADAM17 have shown that binding to the Zn ion lowers the pK_a of the hydroxamic acid and raises the pK_a value of the active site residue Glu406, which results in proton transfer from the hydroxamic acid to Glu406.⁵³ To investigate this event, we performed QM/MM optimizations and rescoring on the 10 complexes containing a hydroxamic acid bound to ADAM17, expanding the QM system to additionally include the side chain of catalytic Glu406. During optimization, in the best clusters of all 10 cases, we observed a proton transfer from the hydroxamic acid to Glu406 (see Figure 8). This highlights an advantage of the QM/MM approach, which is able to dynamically describe this type of chemical reaction.

3.7. Carbonic Anhydrase Results. A striking difference is observed in the success rates for the 65 carbonic anhydrase test cases from the zinc-binding dataset (58.5% classically, 81.5% QM/MM; see Table S2 in the Supporting Information) and

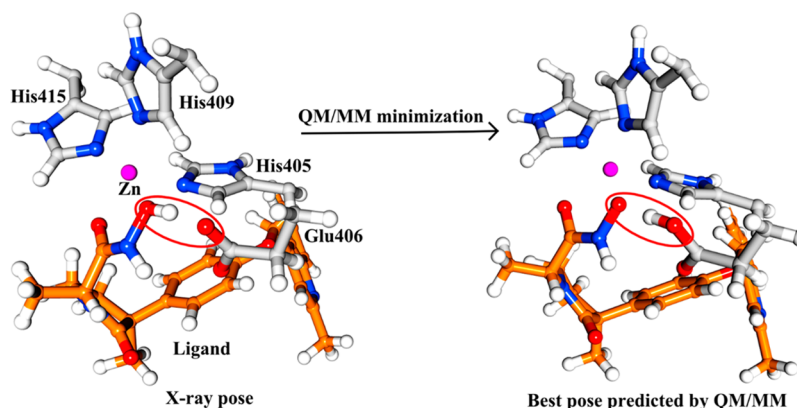


Figure 8. Example of proton transfer event in ADAM17 (PDB ID 2FV5) with expanded QM system including catalytic residue Glu406. The hydroxamic acid ligand (orange) transfers a proton to Glu406 during QM/MM minimization of the X-ray pose.

the 11 test cases from the zinc-nonbinding dataset (0% for both; see Table S3 in the Supporting Information). This difference can mainly be attributed to the different solvent accessibility of the ligands in the two test sets.

The ligands in the zinc-binding dataset are competitive inhibitors that replace the catalytic zinc-bound water molecule and form a direct bond to the Zn ion. In this case, a previous study showed that polarization and charge transfer play an important role.¹⁵ This may explain the higher success rate of the QM/MM scoring function, compared to the classical scoring function. The ligands in the zinc-nonbinding dataset can be divided into two functional types: carbonic anhydrase inhibitors and activators. The inhibitors (for example, coumarin hydrolysis products) block the entrance of the active site.⁸⁹ The activators are also bound at the entrance of the active site and facilitate the catalytic proton-transfer process by participating in an extensive hydrogen-bonding network.⁹⁰ In both cases, the ligands make extensive contact with bulk water, which is reflected in their low burial ($74\% \pm 9\%$). As shown previously, this results in poor performance of both classical and QM/MM scoring (see Figure 3).

4. CONCLUSIONS

In this study, we developed a large high-quality test set of zinc metalloproteins including either competitive or allosteric ligands, which is publicly available and may serve for future benchmarking studies (<http://www.molecular-modelling.ch/resources.php>). We have shown that the allosteric dataset is very valuable for the assessment of the performance of different scoring functions, allowing one to identify overestimated ligand–Zn interactions.

In the classical docking studies, we detected a strong dependence of the success rate on the chosen solvation model. Using the FACTS model, a good success rate was obtained for the zinc-binding dataset (61.5%). Because of difficulties in describing highly solvent accessible ligand conformations, and because of spurious zinc binding, a lower success rate was obtained for the allosteric test set (49.1%). A smart treatment of active site solvation may avoid the latter problem.

Application of the quantum mechanical/molecular mechanical (QM/MM) scoring function with the FACTS solvation model yielded a significantly improved success rate for the zinc-binding dataset (77.0%), while the success rate for the zinc-nonbinding dataset remained constant (49.1%). For the zinc-binding dataset, also the description of correct zinc-binding geometries improved substantially with the hybrid classical/quantum scoring. The use of a QM description of the active site caused a major charge redistribution, resulting in a much reduced positive charge on the Zn ion. Inclusion of the coordinating protein side chains in the QM subsystem proved to be important to describe this charge redistribution and significantly improved the success rate for the allosteric test set. Application of the FACTS solvation model improved docking results, compared to vacuum calculations. In the present test set, geometry optimizations did not improve results when compared to single-point calculations on the classically generated structures. However, this may be different for other metalloproteins, where the ligand–metal interactions are less well-described at the classical level. For some therapeutically relevant enzyme classes, the QM/MM approach yielded substantially higher success rates. In addition, in the case of ADAM17, we could demonstrate that expanding the QM region to the catalytic Glu406 side chain resulted in a proton-

transfer event in the best predicted docking pose, which has been postulated in the literature. The computational cost of the present protocol is substantial when doing extensive geometry optimizations (20.4 h for rescoring 250 binding poses; see Table 4) but low when doing only single-point calculations (0.3 h). A compromise between these two extremes, using different optimization schemes, may be found for different applications.

Comparison to the widely used docking algorithms AutoDock4 and AutoDock Vina under comparable sampling conditions showed that both classical and QM/MM docking with EADock DSS yield higher success rates for the zinc-binding dataset. The QM/MM scoring also performs better for the prediction of correct zinc-binding geometries.

The present results suggest that the increased accuracy of the QM/MM score over a classical scoring scheme can be useful for drug design. In the future, we will fully integrate the presented score into the EADock DSS docking algorithm, allowing for its application to different receptor classes, and we will extend its scope to compare binding free energies of different ligands to different receptors.

■ ASSOCIATED CONTENT

S Supporting Information

Tables with the characteristics of the datasets, the enzyme classification of the complexes, the prediction of zinc-bound complexes, and the prediction of tetrahedral geometries, as well as a figure showing examples of QM/MM docking results. This material is available free of charge via the Internet at <http://pubs.acs.org>.

■ AUTHOR INFORMATION

Corresponding Authors

*E-mail: vincent.zoete@ibz-sib.ch (V. Zoete).

*E-mail: ute.roehrig@ibz-sib.ch (U. F. Röhrig).

Funding

Computational resources were provided by the Vital-IT server of the Swiss Institute of Bioinformatics. This work was supported by Grant No. 135460 to U.R. and V.Z. from the Swiss National Science Foundation.

Notes

The authors declare no competing financial interest.

■ ACKNOWLEDGMENTS

We would like to thank the Vital-IT team of the Swiss Institute of Bioinformatics for providing computational resources. This work was supported by a grant to U.R. and V.Z. from the Swiss National Science Foundation (Grant No. 135460). Molecular graphics were generated using UCSF Chimera (E. F. Pettersen et al., *J. Comput. Chem.* 2004, 25, 1605–1612). Chimera has been developed by the Resource for Biocomputing, Visualization, and Informatics at the University of California, San Francisco (supported by NIGMS No. P41-GM103311). Marvin 6.2, 2013, ChemAxon (<http://www.chemaxon.com>) was used for drawing chemical structures. We would also like to thank Aurélien Grosdidier for technical assistance and Prof. Olivier Michelin for helpful discussions.

■ ABBREVIATIONS

ABNR, adopted basis Newton–Raphson; CHARMM, Chemistry at HARvard Molecular Mechanics; DPI, diffraction-component precision index; FACTS, Fast Analytical Continuum Treatment of Solvation; GBMV2, Generalized Born

Molecular Volume II; Lig-BS, fraction of the ligand surface buried upon complexation; MM, molecular mechanics; QM, quantum mechanics; QM/MM, quantum mechanics/molecular mechanics; SCC-DFTB, self-consistent charge density functional tight binding; SD, steepest descent; SPE, single-point energy; TAng, angle of deviation from ideal tetrahedral geometry

■ REFERENCES

- (1) Jorgensen, W. L. The Many Roles of Computation in Drug Discovery. *Science* **2004**, *303*, 1813–1818.
- (2) Teague, S. J. Implications of Protein Flexibility for Drug Discovery. *Nat. Rev. Drug Discovery* **2003**, *2*, 527–541.
- (3) Shoichet, B. K.; Leach, A. R.; Kuntz, I. D. Ligand Solvation in Molecular Docking. *Proteins: Struct. Funct. Genet.* **1999**, *34*, 4–16.
- (4) Röhrig, U. F.; Grosdidier, A.; Zoete, V.; Michielin, O. Docking to Heme Proteins. *J. Comput. Chem.* **2009**, *30*, 2305–2315.
- (5) Illingworth, C. J. R.; Morris, G. M.; Parkes, K. E. B.; Snell, C. R.; Reynolds, C. A. Assessing the Role of Polarization in Docking. *J. Phys. Chem. A* **2008**, *112*, 12157–12163.
- (6) Warshel, A.; Levitt, M. Theoretical Studies of Enzymic Reactions—Dielectric, Electrostatic and Steric Stabilization of Carbonium-Ion in Reaction of Lysozyme. *J. Mol. Biol.* **1976**, *103*, 227–249.
- (7) Lodola, A.; De Vivo, M. The Increasing Role of QM/MM in Drug Discovery. In *Structural and Mechanistic Enzymology: Bringing Together Experiments and Computing*; Christov, C., Karabencheva-Christova, T., Eds.; Elsevier Academic Press: San Diego, CA, 2012; Vol. 87, pp 337–362.
- (8) Mucs, D.; Bryce, R. A. The Application of Quantum Mechanics in Structure-Based Drug Design. *Expert Opin. Drug Discovery* **2013**, *8*, 263–276.
- (9) Raha, K.; Peters, M. B.; Wang, B.; Yu, N.; WollaCott, A. M.; Westerhoff, L. M.; Merz, K. M. The Role of Quantum Mechanics in Structure-Based Drug Design. *Drug Discovery Today* **2007**, *12*, 725–731.
- (10) Cho, A. E.; Rinaldo, D. Extension of QM/MM Docking and Its Applications to Metalloproteins. *J. Comput. Chem.* **2009**, *30*, 2609–2616.
- (11) Menikarachchi, L. C.; Gascon, J. A. QM/MM Approaches in Medicinal Chemistry Research. *Curr. Top. Med. Chem.* **2010**, *10*, 46–54.
- (12) Zhou, T.; Huang, D.; Caflisch, A. Is Quantum Mechanics Necessary for Predicting Binding Free Energy? *J. Med. Chem.* **2008**, *51*, 4280–4288.
- (13) Zhou, T.; Huang, D. Z.; Caflisch, A. Quantum Mechanical Methods for Drug Design. *Curr. Top. Med. Chem.* **2010**, *10*, 33–45.
- (14) Cho, A. E.; Chung, J. Y.; Kim, M.; Park, K. Quantum Mechanical Scoring for Protein Docking. *J. Chem. Phys.* **2009**, *131*, 134108.
- (15) Raha, K.; Merz, K. M. A Quantum Mechanics-Based Scoring Function: Study of Zinc Ion-Mediated Ligand Binding. *J. Am. Chem. Soc.* **2004**, *126*, 1020–1021.
- (16) Stewart, J. J. P. Application of the PM6 Method to Modeling Proteins. *J. Mol. Model.* **2009**, *15*, 765–805.
- (17) Lepšík, M.; Rezac, J.; Kolar, M.; Pecina, A.; Hobza, P.; Fanfrlik, J. The Semiempirical Quantum Mechanical Scoring Function for in Silico Drug Design. *ChemPlusChem* **2013**, *78*, 921–931.
- (18) Bikadi, Z.; Hazai, E. Application of the PM6 Semi-Empirical Method to Modeling Proteins Enhances Docking Accuracy of Autodock. *J. Cheminf.* **2009**, *1*, 1–15.
- (19) Elstner, M.; Porezag, D.; Jungnickel, G.; Elsner, J.; Haugk, M.; Frauenheim, T.; Suhai, S.; Seifert, G. Self-Consistent-Charge Density-Functional Tight-Binding Method for Simulations of Complex Materials Properties. *Phys. Rev. B* **1998**, *58*, 7260–7268.
- (20) Elstner, M.; Frauenheim, T.; Kaxiras, E.; Seifert, G.; Suhai, S. A Self-Consistent Charge Density-Functional Based Tight-Binding Scheme for Large Biomolecules. *Phys. Status Solidi B* **2000**, *217*, 357–376.
- (21) Cui, Q.; Elstner, M.; Kaxiras, E.; Frauenheim, T.; Karplus, M. A QM/MM Implementation of the Self-Consistent Charge Density Functional Tight Binding (SCC-DFTB) Method. *J. Phys. Chem. B* **2001**, *105*, 569–585.
- (22) Elstner, M.; Cui, Q.; Munih, P.; Kaxiras, E.; Frauenheim, T.; Karplus, M. Modeling Zinc in Biomolecules with the Self Consistent Charge-Density Functional Tight Binding (SCC-DFTB) Method: Applications to Structural and Energetic Analysis. *J. Comput. Chem.* **2003**, *24*, 565–581.
- (23) Elstner, M. The SCC-DFTB Method and Its Application to Biological Systems. *Theor. Chem. Acc.* **2006**, *116*, 316–325.
- (24) Burger, S. K.; Thompson, D. C.; Ayers, P. W. Quantum Mechanics/Molecular Mechanics Strategies for Docking Pose Refinement: Distinguishing between Binders and Decoys in Cytochrome C Peroxidase. *J. Chem. Inf. Model.* **2011**, *51*, 93–101.
- (25) Cho, A. E.; Guallar, V.; Berne, B. J.; Friesner, R. Importance of Accurate Charges in Molecular Docking: Quantum Mechanical/Molecular Mechanical (QM/MM) Approach. *J. Comput. Chem.* **2005**, *26*, 915–931.
- (26) Illingworth, C. J. R.; Parkes, K. E. B.; Snell, C. R.; Ferenczy, G. G.; Reynolds, C. A. Toward a Consistent Treatment of Polarization in Model QM/MM Calculations. *J. Phys. Chem. A* **2008**, *112*, 12151–12156.
- (27) Englebienne, P.; Fiaux, H.; Kuntz, D. A.; Corbeil, C. R.; Gerber-Lemaire, S.; Rose, D. R.; Moitessier, N. Evaluation of Docking Programs for Predicting Binding of Golgi Alpha-Mannosidase II Inhibitors: A Comparison with Crystallography. *Proteins* **2007**, *69*, 160–176.
- (28) Beierlein, F.; Lanig, H.; Schurer, G.; Horn, A. H. C.; Clark, T. Quantum Mechanical/Molecular Mechanical (QM/MM) Docking: An Evaluation for Known Test Systems. *Mol. Phys.* **2003**, *101*, 2469–2480.
- (29) Khandelwal, A.; Lukacova, V.; Comez, D.; Kroll, D. M.; Raha, S.; Balaz, S. A Combination of Docking, QM/MM Methods, and MD Simulation for Binding Affinity Estimation of Metalloprotein Ligands. *J. Med. Chem.* **2005**, *48*, 5437–5447.
- (30) Raha, K.; Merz, K. M. Large-Scale Validation of a Quantum Mechanics Based Scoring Function: Predicting the Binding Affinity and the Binding Mode of a Diverse Set of Protein–Ligand Complexes. *J. Med. Chem.* **2005**, *48*, 4558–4575.
- (31) Soderhjelm, P.; Kongsted, J.; Ryde, U. Ligand Affinities Estimated by Quantum Chemical Calculations. *J. Chem. Theory Comput.* **2010**, *6*, 1726–1737.
- (32) Soderhjelm, P.; Kongsted, J.; Genheden, S.; Ryde, U. Estimates of Ligand-Binding Affinities Supported by Quantum Mechanical Methods. *Interdiscip. Sci.–Comput. Life Sci.* **2010**, *2*, 21–37.
- (33) Hayik, S. A.; Dunbrack, R., Jr.; Merz, K. M., Jr. Mixed Quantum Mechanics/Molecular Mechanics Scoring Function to Predict Protein–Ligand Binding Affinity. *J. Chem. Theory Comput.* **2010**, *6*, 3079–3091.
- (34) Wang, J. C.; Lin, J. H.; Chen, C. M.; Perryman, A. L.; Olson, A. J. Robust Scoring Functions for Protein–Ligand Interactions with Quantum Chemical Charge Models. *J. Chem. Inf. Model.* **2011**, *51*, 2528–2537.
- (35) Natesan, S.; Subramaniam, R.; Bergeron, C.; Balaz, S. Binding Affinity Prediction for Ligands and Receptors Forming Tautomers and Ionization Species: Inhibition of Mitogen-Activated Protein Kinase-Activated Protein Kinase 2 (MK2). *J. Med. Chem.* **2012**, *55*, 2035–2047.
- (36) Mikulskis, P.; Genheden, S.; Wichmann, K.; Ryde, U. A Semiempirical Approach to Ligand-Binding Affinities: Dependence on the Hamiltonian and Corrections. *J. Comput. Chem.* **2012**, *33*, 1179–1189.
- (37) Fong, P.; McNamara, J. P.; Hillier, I. H.; Bryce, R. A. Assessment of QM/MM Scoring Functions for Molecular Docking to HIV-1 Protease. *J. Chem. Inf. Model.* **2009**, *49*, 913–924.
- (38) Khandelwal, A.; Balaz, S. QM/MM Linear Response Method Distinguishes Ligand Affinities for Closely Related Metalloproteins. *Proteins* **2007**, *69*, 326–339.

- (39) Brooks, B. R.; Brooks, C. L.; Mackerell, A. D.; Nilsson, L.; Petrella, R. J.; Roux, B.; Won, Y.; Archontis, G.; Bartels, C.; Boresch, S.; Caflisch, A.; Caves, L.; Cui, Q.; Dinner, A. R.; Feig, M.; Fischer, S.; Gao, J.; Hodoscek, M.; Im, W.; Kuczera, K.; Lazaridis, T.; Ma, J.; Ovchinnikov, V.; Paci, E.; Pastor, R. W.; Post, C. B.; Pu, J. Z.; Schaefer, M.; Tidor, B.; Venable, R. M.; Woodcock, H. L.; Wu, X.; Yang, W.; York, D. M.; Karplus, M. CHARMM: The Biomolecular Simulation Program. *J. Comput. Chem.* **2009**, *30*, 1545–1614.
- (40) Grosdidier, A.; Zoete, V.; Michielin, O. Fast Docking Using the CHARMM Force Field with Eadock DSS. *J. Comput. Chem.* **2011**, *32*, 2149–2159.
- (41) Lee, Y. M.; Lim, C. Physical Basis of Structural and Catalytic Zn-Binding Sites in Proteins. *J. Mol. Biol.* **2008**, *379*, 545–553.
- (42) McCall, K. A.; Huang, C. C.; Fierke, C. A. Function and Mechanism of Zinc Metalloenzymes. *J. Nutr.* **2000**, *130*, 1437S–1446S.
- (43) Jacobsen, F. E.; Lewis, J. A.; Cohen, S. M. The Design of Inhibitors for Medicinally Relevant Metalloproteins. *ChemMedChem* **2007**, *2*, 152–171.
- (44) Anzellotti, A. I.; Farrell, N. P. Zinc Metalloproteins as Medicinal Targets. *Chem. Soc. Rev.* **2008**, *37*, 1629–1651.
- (45) Li, Y. L.; Mei, Y.; Zhang, D. W.; Xie, D. Q.; Zhang, J. Z. H. Structure and Dynamics of a Dizinc Metalloprotein: Effect of Charge Transfer and Polarization. *J. Phys. Chem. B* **2011**, *115*, 10154–10162.
- (46) Donini, O. A. T.; Kollman, P. A. Calculation and Prediction of Binding Free Energies for the Matrix Metalloproteinases. *J. Med. Chem.* **2000**, *43*, 4180–4188.
- (47) Tuccinardi, T.; Martinelli, A.; Nuti, E.; Carelli, P.; Balzano, F.; Uccello-Barretta, G.; Murphy, G.; Rossello, A. Amber force field implementation, molecular modelling study, synthesis and MMP-1/MMP-2 inhibition profile of (R) and (S)-N-hydroxy-2-(N-isopropoxybiphenyl-4-ylsulfonamido)-3-methylbutanamides. *Bioorg. Med. Chem.* **2006**, *14*, 4260–4276.
- (48) Hu, X.; Balaz, S.; Shelver, W. H. A Practical Approach to Docking of Zinc Metalloproteinase Inhibitors. *J. Mol. Graph.* **2004**, *22*, 293–307.
- (49) Ferrara, P.; Gohlke, H.; Price, D. J.; Klebe, G.; Brooks, C. L. Assessing Scoring Functions for Protein-Ligand Interactions. *J. Med. Chem.* **2004**, *47*, 3032–3047.
- (50) Grosdidier, A.; Zoete, V.; Michielin, O. Blind Docking of 260 Protein–Ligand Complexes with Eadock 2.0. *J. Comput. Chem.* **2009**, *30*, 2021–2030.
- (51) Santos-Martins, D.; Forli, S.; Ramos, M. J.; Olson, A. J. AutoDock4Zn: An Improved Autodock Force Field for Small-Molecule Docking to Zinc Metalloproteins. *J. Chem. Inf. Model.* **2014**, *54*, 2371–9.
- (52) Goto, J.; Kataoka, R.; Hirayama, N. Ph4Dock: Pharmacophore-Based Protein–Ligand Docking. *J. Med. Chem.* **2004**, *47*, 6804–6811.
- (53) Cross, J. B.; Duca, J. S.; Kaminski, J. J.; Madison, V. S. The Active Site of a Zinc-Dependent Metalloproteinase Influences the Computed pK(a)s of Ligands Coordinated to the Catalytic Zinc Ion. *J. Am. Chem. Soc.* **2002**, *124*, 11004–11007.
- (54) Pottel, J.; Therrien, E.; Gleason, J. L.; Moitessier, N. Docking Ligands into Flexible and Solvated Macromolecules. 6. Development and Application to the Docking of Hdacs and Other Zinc Metalloenzymes Inhibitors. *J. Chem. Inf. Model.* **2014**, *54*, 254–265.
- (55) Bernstein, F. C.; Koetzle, T. F.; Williams, G. J. B.; Meyer, E. F.; Brice, M. D.; Rodgers, J. R.; Kennard, O.; Shimanouchi, T.; Tasumi, M. Protein Data Bank—Computer-Based Archival File for Macromolecular Structures. *J. Mol. Biol.* **1977**, *112*, 535–542.
- (56) Warren, G. L.; Do, T. D.; Kelley, B. P.; Nicholls, A.; Warren, S. D. Essential Considerations for Using Protein-Ligand Structures in Drug Discovery. *Drug Discovery Today* **2012**, *17*, 1270–1281.
- (57) Zoete, V.; Cuendet, M. A.; Grosdidier, A.; Michielin, O. SwissParam: A Fast Force Field Generation Tool for Small Organic Molecules. *J. Comput. Chem.* **2011**, *32*, 2359–2368.
- (58) Stewart, J. J. P. Optimization of Parameters for Semiempirical Methods V: Modification of Nddo Approximations and Application to 70 Elements. *J. Mol. Model.* **2007**, *13*, 1173–1213.
- (59) Zheng, G. S.; Witek, H. A.; Bobadova-Parvanova, P.; Irle, S.; Musaev, D. G.; Prabhakar, R.; Morokuma, K. Parameter Calibration of Transition-Metal Elements for the Spin-Polarized Self-Consistent-Charge Density-Functional Tight-Binding (DFTB) Method: Sc, Ti, Fe, Co, and Ni. *J. Chem. Theory Comput.* **2007**, *3*, 1349–1367.
- (60) Moreira, N. H.; Dolgonos, G.; Aradi, B.; da Rosa, A. L.; Frauenheim, T. Toward an Accurate Density-Functional Tight-Binding Description of Zinc-Containing Compounds. *J. Chem. Theory Comput.* **2009**, *5*, 605–614.
- (61) Pettersen, E. F.; Goddard, T. D.; Huang, C. C.; Couch, G. S.; Greenblatt, D. M.; Meng, E. C.; Ferrin, T. E. UCSF Chimera—A Visualization System for Exploratory Research and Analysis. *J. Comput. Chem.* **2004**, *25*, 1605–1612.
- (62) El Yazal, J.; Pang, Y. P. Proton Dissociation Energies of Zinc-Coordinated Hydroxamic Acids and Their Relative Affinities for Zinc: Insight into Design of Inhibitors of Zinc-Containing Proteinases. *J. Phys. Chem. B* **2000**, *104*, 6499–6504.
- (63) Halgren, T. A.; Bush, B. L. The Merck Molecular Force Field (MMFF94). Extension and Application. *Abstr. Pap. Am. Chem. Soc.* **1996**, *212*, 2-COMP.
- (64) MacKerell, A. D.; Bashford, D.; Bellott, M.; Dunbrack, R. L.; Evanseck, J. D.; Field, M. J.; Fischer, S.; Gao, J.; Guo, H.; Ha, S.; Joseph McCarthy, D.; Kuchnir, L.; Kuczera, K.; Lau, F. T. K.; Mattos, C.; Michnick, S.; Ngo, T.; Nguyen, D. T.; Prodhom, B.; Reiher, W. E.; Roux, B.; Schlenkrich, M.; Smith, J. C.; Stote, R.; Straub, J.; Watanabe, M.; Wiorkiewicz-Kuczera, J.; Yin, D.; Karplus, M. All-Atom Empirical Potential for Molecular Modeling and Dynamics Studies of Proteins. *J. Phys. Chem. B* **1998**, *102*, 3586–3616.
- (65) MacKerell, A. D. Developments in the CHARMM All-Atom Empirical Energy Function for Biological Molecules. *Abstr. Pap. Am. Chem. Soc.* **1998**, *216*, U696–U696.
- (66) Mackerell, A. D. Empirical Force Fields for Biological Macromolecules: Overview and Issues. *J. Comput. Chem.* **2004**, *25*, 1584–1604.
- (67) Stote, R. H.; Karplus, M. Zinc-Binding in Proteins and Solution—A Simple but Accurate Nonbonded Representation. *Proteins: Struct. Funct. Genet.* **1995**, *23*, 12–31.
- (68) Grosdidier, A.; Zoete, V.; Michielin, O. SwissDock, a Protein–Small Molecule Docking Web Service Based on Eadock DSS. *Nucleic Acids Res.* **2011**, *39*, W270–W277.
- (69) Zoete, V.; Grosdidier, A.; Cuendet, M.; Michielin, O. Use of the FACTS Solvation Model for Protein–Ligand Docking Calculations. Application to Eadock. *J. Mol. Recognit.* **2010**, *23*, 457–461.
- (70) Haberthur, U.; Caflisch, A. FACTS: Fast Analytical Continuum Treatment of Solvation. *J. Comput. Chem.* **2008**, *29*, 701–715.
- (71) Lee, M. S.; Feig, M.; Salsbury, F. R.; Brooks, C. L. New Analytic Approximation to the Standard Molecular Volume Definition and Its Application to Generalized Born Calculations. *J. Comput. Chem.* **2003**, *24*, 1348–1356.
- (72) Morris, G. M.; Huey, R.; Lindstrom, W.; Sanner, M. F.; Belew, R. K.; Goodsell, D. S.; Olson, A. J. AutoDock4 and AutoDockTools4: Automated Docking with Selective Receptor Flexibility. *J. Comput. Chem.* **2009**, *30*, 2785–2791.
- (73) Huey, R.; Morris, G. M.; Olson, A. J.; Goodsell, D. S. A Semiempirical Free Energy Force Field with Charge-Based Desolvation. *J. Comput. Chem.* **2007**, *28*, 1145–1152.
- (74) Trott, O.; Olson, A. J. Software News and Update Autodock Vina: Improving the Speed and Accuracy of Docking with a New Scoring Function, Efficient Optimization, and Multithreading. *J. Comput. Chem.* **2010**, *31*, 455–461.
- (75) Morris, G. M.; Goodsell, D. S.; Halliday, R. S.; Huey, R.; Hart, W. E.; Belew, R. K.; Olson, A. J. Automated Docking Using a Lamarckian Genetic Algorithm and an Empirical Binding Free Energy Function. *J. Comput. Chem.* **1998**, *19*, 1639–1662.
- (76) Mobley, D. L.; Guthrie, J. P. Freesolv: A Database of Experimental and Calculated Hydration Free Energies, with Input Files. *J. Comput.-Aided Mol. Des.* **2014**, *28*, 711–720.
- (77) Rocks, N.; Paulissen, G.; El Hour, M.; Quesada, F.; Crahay, C.; Gueders, M.; Foidart, J. M.; Noel, A.; Cataldo, D. Emerging Roles of

- ADAM and ADAMTS Metalloproteinases in Cancer. *Biochimie* **2008**, *90*, 369–379.
- (78) Rowan, A. D.; Litherland, G. J.; Hui, W.; Milner, J. M. Metalloproteases as Potential Therapeutic Targets in Arthritis Treatment. *Expert Opin. Ther. Targets* **2008**, *12*, 1–18.
- (79) Moss, M. L.; White, J. M.; Lambert, M. H.; Andrews, R. C. TACE and Other ADAM Proteases as Targets for Drug Discovery. *Drug Discovery Today* **2001**, *6*, 417–426.
- (80) Lovering, F.; Zhang, Y. Therapeutic Potential of TACE Inhibitors in Stroke. *Curr. Drug Targets—CNS Neurol. Disord.* **2005**, *4*, 161–168.
- (81) Yang, P.; Baker, K. A.; Hagg, T. The ADAMS Family: Coordinators of Nervous System Development, Plasticity and Repair. *Prog. Neurobiol.* **2006**, *79*, 73–94.
- (82) van den Elsen, J. M. H.; Kuntz, D. A.; Rose, D. R. Structure of Golgi Alpha-Mannosidase II: A Target for Inhibition of Growth and Metastasis of Cancer Cells. *EMBO J.* **2001**, *20*, 3008–3017.
- (83) Supuran, C. T.; Scozzafava, A. Carbonic Anhydrase Inhibitors—Part 94. 1,3,4-Thiadiazole-2-Sulfonamide Derivatives as Antitumor Agents? *Eur. J. Med. Chem.* **2000**, *35*, 867–874.
- (84) Scozzafava, A.; Supuran, C. T. Glaucoma and the Applications of Carbonic Anhydrase Inhibitors. *Subcell. Biochem.* **2014**, *75*, 349–359.
- (85) Kemp, L. E.; Bond, C. S.; Hunter, W. N. Structure of 2C-Methyl-D-Erythritol 2,4-Cyclodiphosphate Synthase: An Essential Enzyme for Isoprenoid Biosynthesis and Target for Antimicrobial Drug Development. *Proc. Natl. Acad. Sci. U. S. A.* **2002**, *99*, 6591–6596.
- (86) MacLean, J. K. F.; Leese, D. N.; Leslie, B. W.; Olusanya, O. A.; Riddell, M. P.; Webster, S. P.; Zhao, L. The Non-Mevalonate Pathway Enzyme 2C-methyl-D-erythritol-2,4-cyclodiphosphate synthase as a Novel Target for Antimicrobial Chemotherapy. *Abstr. Intersci. Conf. Antimicrob. Agents Chemother.* **2003**, *43*, 220.
- (87) Yang, Y.; Lightstone, F. C.; Wong, S. E. Approaches to Efficiently Estimate Solvation and Explicit Water Energetics in Ligand Binding: The Use of WaterMap. *Expert Opin. Drug Discovery* **2013**, *8*, 277–287.
- (88) Hou, G.; Zhu, X.; Cui, Q. An Implicit Solvent Model for SCC-DFTB with Charge-Dependent Radii. *J. Chem. Theory Comput.* **2010**, *6*, 2303–2314.
- (89) Maresca, A.; Temperini, C.; Vu, H.; Pham, N. B.; Poulsen, S.-A.; Scozzafava, A.; Quinn, R. J.; Supuran, C. T. Non-Zinc Mediated Inhibition of Carbonic Anhydrases: Coumarins Are a New Class of Suicide Inhibitors. *J. Am. Chem. Soc.* **2009**, *131*, 3057–3062.
- (90) Bhatt, D.; Fisher, S. Z.; Tu, C.; McKenna, R.; Silverman, D. N. Location of Binding Sites in Small Molecule Rescue of Human Carbonic Anhydrase II. *Biophys. J.* **2007**, *92*, 562–570.